Xanthomonas type III effector XopN targets scaffold protein OsRACK1B to suppress rice immunity

Jiuxiang Wang[1,3,*], Zhe Ni[1,2,*], Xin Chen[1], Yaqi Zhang[1], Huajun Qin[1], Haoyu Wang[1], Yongqiang He[1,3], Jiliang Tang[1], Sheng Huang[1]

[1]State Key Laboratory for Conservation and Utilization of Subtropical Agro-bioresources, College of Life Science and Technology, Guangxi University, Nanning 530004, Guangxi, China

[2]College of Plant Protection, Northeast Agricultural University, Harbin 150030, Harbin, China

[3]College of Agriculture, Guangxi University, Nanning 530004, Guangxi, China

Author for correspondence:

Sheng Huang

Tel: +8618076635685

Email: shuang@gxu.edu.cn

*These authors contributed equally to this work.

Summary

Bacterial leaf streak (BLS), caused by *Xanthomonas oryzae* pv. *oryzicola* (*Xoc*), is a major bacterial disease that poses a substantial threat to rice production. Although *Xoc* deploys a variety of non-transcription activator-like (non-TAL) effectors to subvert host defenses, the mechanistic basis of how these effectors modulate plant immune signaling remains largely unclear.

Through yeast two-hybrid screening, we identified the rice scaffold protein OsRACK1B as a host target of *Xoc* effector XopN, and its potential role during

Xoc infection was characterized by combining gene function with biochemical analyses.

We demonstrate that XopN suppresses rice immune responses and physically interacts with the rice scaffold protein OsRACK1B. Notably, OsRACK1B expression is induced following *Xoc* infection in a type III secretion system (T3SS)-independent manner. Functional analyses indicate that *OsRACK1B* overexpression enhances *Xoc* resistance, whereas loss-of-function mutants exhibit heightened susceptibility. This increased susceptibility is characterized by compromised immunity, including reduced callose deposition, diminished reactive oxygen species (ROS) accumulation, and attenuated expression of defense-related genes such as *OsPBZ1* and *OsPAL1*. Furthermore, XopN competes with OsRap2.6 for binding to OsRACK1B, thereby disrupting the formation of the OsRACK1B – OsRap2.6 immune complex.

Our findings reveal a novel virulence strategy employed by *Xoc*, in which XopN targets and disrupts OsRACK1B-mediated immune signaling, thereby compromising host defense.

Keywords: *Xanthomonas oryzae* pv. *oryzicola*; rice; non-TAL effectors; scaffold protein; immune responses

Introduction

Rice (*Oryza sativa* L.) is a staple crop that sustains the nutritional demands of more than half of the global population (Yuan *et al.*, 2021). However, its productivity is continually threatened by a diverse array of pathogens and pests, which compromise both yield and grain quality (He *et al.*, 2023). Among these, bacterial leaf streak (BLS), caused by *Xanthomonas oryzae* pv. *oryzicola* (*Xoc*), is a major bacterial disease that results in yield losses ranging from 8% to 32% (Liu *et al.*, 2014). Genetically encoded resistance remains the most effective

52 and environmentally sustainable approach for long-term disease management.
53 Despite progress, only a limited number of resistance (*R*) genes, such as *Xo1*,
54 *xa5*, *bls1*, and *OsBLS6.2*, have been identified as effective against BLS. (Xie *et*
55 *al.*, 2014; Triplett *et al.*, 2016; Ma *et al.*, 2021; Xie *et al.*, 2023). This underscores
56 the pressing need to elucidate the molecular strategies employed by *Xoc* to
57 facilitate infection, which will be instrumental for the development of novel
58 resistance traits.

59 The continuous co-evolution of pathogenic microbes and their host plants
60 has led to the emergence of a sophisticated, two-layered innate immune system
61 in plants: pattern-triggered immunity (PTI) and effector-triggered immunity (ETI)
62 (Jones & Dangl, 2006; Wang *et al.*, 2022). PTI is initiated upon recognition of
63 conserved pathogen-associated molecular patterns (PAMPs) by pattern
64 recognition receptors (PRRs) located at the plasma membrane (Li *et al.*, 2016).
65 In contrast, ETI is activated intracellularly through nucleotide-binding leucine-
66 rich repeat (NLR) receptors that detect pathogen-secreted effectors (Tsuda &
67 Katagiri, 2010). Immune activation induces a range of defense responses,
68 including the production of reactive oxygen species (ROS), callose deposition,
69 mitogen-activated protein kinase (MAPK) cascade activation, upregulation of
70 defense-related genes, and hypersensitive cell death (HR) at the site of
71 infection (Spoel & Dong, 2012; Wang *et al.*, 2020; Gao *et al.*, 2021). While PTI
72 provides basal immunity, ETI elicits a more robust and rapid defense, often
73 accompanied by localized cell death to restrict pathogen spread (Spoel & Dong,
74 2012).

75 Many bacterial phytopathogens utilize a type III secretion system (T3SS) to
76 translocate type III-secreted effectors (T3SEs) directly into host cells, where
77 they manipulate host immunity and facilitate colonization (Boller & He, 2009).
78 In *Xanthomonas* species, T3SEs are broadly classified into transcription
79 activator-like (TAL) effectors and non-TAL effectors (Kay & Bonas, 2009). TAL
80 effectors function as transcriptional activators upon nuclear import, often

reprogramming host gene expression to support bacterial growth. For instance, TAL effectors from *X. oryzae* pv. *oryzae* (*Xoo*) induce *OsSWEET* gene expression, enabling pathogen exploitation of host sugars (Oliva *et al.*, 2019). Similarly, the TAL effector Tal2g from *Xoc* promotes disease by upregulating the sulfate transporter gene *OsSULTR3;6* (Cernadas *et al.*, 2014).

By contrast, non-TAL effectors exploit a diverse array of biochemical strategies to reprogram host cellular processes and facilitate bacterial colonization. For example, *X. campestris* pv. *vesicatoria* (*Xcv*) effector XopL functions as an E3 ubiquitin ligase that interacts with and degrades the autophagy component SH3P2, thereby promoting infection (Leong *et al.*, 2022). Another effector, XopR from *X. campestris* pv. *campestris* (*Xcc*), forms biomolecular condensates via electrostatic-driven liquid–liquid phase separation (LLPS), coacervating with formin-mediated actin nucleation complexes and manipulating the host cytoskeleton (Sun *et al.*, 2021). Recent studies have increasingly highlighted the functional diversity of non-TAL effectors deployed by *Xoc*. For instance, XopC2 acts as a kinase that phosphorylates the Skp1 protein OSK1, thereby suppressing immune signaling (Wang *et al.*, 2021). The effector AvrRxo1 degrades the pyridoxal phosphate synthase OsPDX1, reducing vitamin B6 levels and suppressing stomatal immunity (Liu, H *et al.*, 2022). XopAP competitively binds phosphatidylinositol 3,5-bisphosphate (PtdIns(3,5)P2), inhibiting vacuolar acidification by interfering with vacuolar H^+-pyrophosphatase (V-PPase), ultimately promoting stomatal opening(Liu, L *et al.*, 2022). More recently, XopAK was shown to repress *OsMYBxoc1* transcription and alter host iron homeostasis, thereby modulating rice immunity (Zhang *et al.*, 2024).

Several non-TAL effectors, including AvrBs2, hrpE3 and XopN, have been identified as critical for the full virulence of *Xoc* (Cui *et al.*, 2013; Li *et al.*, 2015; Liao *et al.*, 2020). However, the molecular mechanisms by which these effectors contribute to pathogenicity in rice remain largely unknown. Our previous study

110 established that XopN significantly enhances the virulence of the *Xoc* strain
111 GX01 (Liao *et al.*, 2020). Here, we demonstrate that XopN suppresses rice
112 immune responses and identify the rice scaffold protein OsRACK1B as a novel
113 host target of XopN. Mechanistically, XopN impairs OsRACK1B function by
114 disrupting its association with the transcription factor OsRap2.6, thereby
115 dismantling a critical immune signaling complex. Functional analyses revealed
116 that overexpression of *OsRACK1B* enhances rice resistance to *Xoc*, whereas
117 *OsRACK1B* knockout lines exhibit heightened susceptibility and impaired
118 immune responses. Collectively, these findings highlight a virulence strategy
119 whereby XopN targets a central immune scaffold to suppress host defense,
120 highlighting OsRACK1B as a promising molecular target for breeding BLS-
121 resistant rice varieties.

122 **Materials and Methods**

123 **Plants and bacterial strains**

124 Rice cultivar Nipponbare was used as the wild-type (WT) control in this study.
125 For the overexpression of OsRACK1B, its coding sequence was PCR-amplified
126 and cloned into the pCAMBIA1301-HA binary vector. To generate knockout
127 lines, two guide RNAs targeting the coding region of OsRACK1B were designed
128 using the CRISPR-GE online toolkit (Xie *et al.*, 2017). The gRNA expression
129 cassettes were subsequently inserted into the pYLCRISPR/Cas9 binary vector.
130 Both overexpression and CRISPR constructs were introduced into *Nipponbare*
131 via *A. tumefaciens*-mediated transformation (Wuhan BioRun Biosciences Co.,
132 Ltd.). Rice plants were cultivated in greenhouse conditions under a 14-hour light
133 (30°C)/10-hour dark (28°C) photoperiod.

134 *E. coli* and *A. tumefaciens* strains were propagated in LB medium at 37°C
135 and 28°C, respectively. *Xoc* strains were cultured at 28°C in NB medium
136 (polypeptone 5g/L, beef paste 3g/L, yeast extract 1g/L, sucrose 10g/L).

137 Virulence assays were conducted as previously described (Wang *et al.*, 2024).
138 Briefly, *Xoc* strains were resuspended in sterile distilled water to an optical
139 density of OD_{600} = 0.5 and infiltrated into rice leaves using needleless syringes.
140 Lesion lengths were recorded, and photographs were taken 14 days post-
141 inoculation.

142 **RNA analysis**

143 Total RNA was extracted from rice leaf tissue using TRIzol Reagent (Invitrogen,
144 Cat# 15596018, USA) according to the manufacturer's protocol. First-strand
145 cDNA synthesis was performed with the RevertAid First Strand cDNA Synthesis
146 Kit (Thermo Fisher Scientific, Cat# K1622, USA). Quantitative real-time PCR
147 (RT-qPCR) was conducted using the qTOWER 2.2 Real-Time PCR Detection
148 System (Analytik Jena, Germany) with ChamQ SYBR Color qPCR Master Mix
149 (Vazyme, Cat# Q411-02, China), following the manufacturer's instructions.
150 OsACTIN1 was used as the internal reference gene to normalize transcript
151 levels. Relative gene expression was calculated using the $2^{-\Delta\Delta CT}$ method.
152 Primer sequences used in this study are listed in Table S1.

153 **Callose deposition and DAB staining**

154 Leaves from 2–3-week-old rice seedlings inoculated with *Xoc* were fixed in
155 ethanol: acetic acid (3:1, v/v) for 5 h, with frequent replacement of the solution
156 until fully decolorized. Samples were subsequently rehydrated through a
157 graded ethanol series (70% for 2 h, 50% for 2 h), followed by incubation in
158 distilled water overnight. After triple rinsing with water, the tissues were cleared
159 by incubation in 10% (w/v) NaOH for 1 h. Leaves were then washed four times
160 with water and stained in 0.01% aniline blue solution (150 mM K_2HPO_4, pH 9.5)
161 for 4 h. Callose deposits were visualized immediately using a fluorescence
162 microscope equipped with a UV filter(Deb *et al.*, 2020).

163 For DAB staining, inoculated rice leaves were collected and incubated in DAB

solution (1 mg/mL, Sigma Aldrich) for 24 h with gentle agitation. Leaves were subsequently cleared in a decolorizing solution composed of ethanol, acetic acid, and glycerol (3:1:1, v/v/v) before imaging(Deb *et al.*, 2020).

Y2H assay and Y3H assay

The Matchmaker gold Y2H system (Clontech) was used to screen XopN-interacting proteins. The XopN coding sequence was cloned into the bait vector pGBKT7 and then transformed into the yeast strain Y2H gold. A rice cDNA library was constructed into the prey vector pGADT7 using mRNA extracted from rice leaves according to the manufacturer's protocol. Positive interactors were initially selected on SD/-Leu/-Trp/-His/-Ade dropout medium. To validate the interaction between XopN and OsRACK1B, their coding sequences were individually cloned into pGBKT7 and pGADT7, respectively, and co-transformed into the Y2HGold strain. Transformed yeast colonies were selected on SD/-Leu/-Trp plates, and interactions were assessed by growth on quadruple dropout medium (SD/-Leu/-Trp/-His/-Ade).

For the Y3H assay, the pBridge vector was used to express both XopN and OsRACK1B. The pGADT7 vector was used to express OsRap2.6. The recombinant constructs were co-transformed into the yeast strain Y2HGold. Transformants were selected on SD/-Met/-Trp/-Leu medium, and protein–protein interactions were assessed by growth on SD/-Met/-Trp/-Leu/-His/-Ade selective plates.

Pull-down assay

The XopN coding sequence was cloned into the vector pET28a to generate His-XopN fusion protein. The coding sequence of OsRACK1B was cloned into the vector pGEX-6p-1 to generate GST-OsRACK1B fusion protein. His-XopN and GST-OsRACK1B were expressed in *E. coli* strain BL21 and were purified with Ni-NTA resin and GST resin, respectively (Transgen). His-XopN proteins were

191 immobilized on Ni-NTA resin and incubated with GST-OsRACK1B or GST at
192 4°C for 4 h with gentle shaking. After five times washing with 1 × PBS (4.2 mM
193 Na_2HPO_4, 2 mM KH_2PO_4, 140 mM NaCl, and 10 mM KCl), the mixtures were
194 eluted using the elution buffer. Last, the elution samples were boiled with 5 ×
195 SDS loading buffer at 100°C for 5 min for immunoblot analysis.

196 **BIFC assay**

197 The pXY104 and pXY106 plasmids were used for the BIFC assay. The coding
198 sequence of XopN was cloned into pXY106 to make the XopN-nYFP fusion
199 protein. The OsRACK1B coding sequence was cloned into pXY104 to make
200 the OsRACK1B-cYFP fusion protein. The constructs were co-expressed in rice
201 protoplasts. The YFP fluorescence was observed using a confocal laser
202 scanning microscope (Leica TCS SP8 MP).

203 **Subcellular localization**

204 To examine the subcellular location of XopN and OsRACK1B, full-length cDNAs
205 were constructed into vector pBWA(V)HS-GFP and pBWA(V)HS-GFP to make
206 the fusion proteins XopN-GFP and OsRACK1B-CF, respectively. The
207 recombinant plasmids were transfected into rice protoplasts, and the
208 fluorescence was observed using a confocal laser scanning microscope at 24
209 h after transfection.

210 **Sequence alignment and phylogenetic analysis**

211 Orthologs of XopN from various bacterial species were identified and retrieved
212 from the NCBI database. Protein sequences were aligned using the Constraint-
213 based Multiple Alignment Tool (COBALT), and the resulting alignments were
214 visualized with the online software ESPript 3.0 (Robert & Gouet, 2014). NCBI
215 BLASTP was used to select and download the orthologs of OsRACK1B in other
216 plants. A phylogenetic tree was constructed with MEGA 7.0 using the maximum
217 likelihood (ML) method and 1,000 bootstrap replicates.

218 **Accession numbers**

219 The sequence data from this article can be found on the Kyoto Encyclopedia of
220 Genes and Genomes website (https://www.kegg.jp/) under the following
221 numbers: *xopN* (*Xoc_0350*), *OsRACK1B* (*Os05g0552300*), *OsPBZ1*
222 (*Os12g0555500*), *OsPAL1* (*Os02g0626100*), *OsRap2.6* (*Os04g0398000*) and
223 *OsACTIN* (*Os03g0718100*).

224 Results

225 **Δ*xopN* mutant elicits elevated rice immune responses**

226 To gain insights into the evolutionary conservation of XopN, we performed a
227 BLAST analysis using its amino acid sequence as a query. The results revealed
228 that XopN is highly conserved within the *Xanthomonas* genus, exhibiting 96.0%
229 sequence identity with its homolog in *Xoo*, 81.7% identity with the counterpart
230 in *Xcc*, and 60.9% identity with the homolog in *Xcv* (Fig. S1). Notably, a putative
231 homolog sharing 52.5% identity was also identified in *Acidovorax citrulli*, a
232 vascular pathogen of cucurbits, suggesting potential horizontal conservation
233 beyond the *Xanthomonas* clade. In contrast, XopN shows limited sequence
234 similarity to effector-like proteins from more distantly related phytopathogens,
235 such as *Ralstonia solanacearum* (25.2% identity), indicating that XopN and its
236 functional equivalents are largely restricted to *Xanthomonas* and a few
237 phylogenetically proximate taxa.

238 We further investigated the functional role of the *Xoc* effector XopN in
239 modulating rice innate immunity by comparing host responses triggered by the
240 wild-type strain GX01, the Δ*xopN* mutant, and the complemented strain
241 CΔ*xopN*. Callose, a β-1,3-glucan polymer, serves as a critical component of
242 plant immune defenses by reinforcing cell walls to restrict pathogen ingress and
243 dissemination (Li *et al.*, 2023). Accordingly, we first assessed callose deposition
244 in rice leaves infiltrated with GX01, Δ*xopN*, or CΔ*xopN*. The results revealed

245 that leaves infected with the Δ*xopN* mutant exhibited significantly enhanced
246 callose accumulation relative to those inoculated with either GX01 or CΔ*xopN*
247 (Fig. 1a,b). We next assessed ROS production, a rapid defense response
248 typically associated with PTI activation. Using 3,3′-diaminobenzidine (DAB)
249 staining, we observed a marked increase in H_2O_2 accumulation in Δ*xopN*-
250 infected leaves compared to those infected with GX01 or CΔ*xopN* (Fig. 1c). To
251 determine whether XopN also modulates transcriptional defense responses, we
252 conducted quantitative reverse transcription PCR (RT–qPCR) to analyze the
253 transcript levels of canonical defense marker genes. The expression of
254 *OsPBZ1* and *OsPAL1* was significantly upregulated in Δ*xopN*-infected leaves
255 compared to GX01 (Fig. 1d,e), indicating that XopN suppresses transcriptional
256 activation of these defense-associated genes.

257 Effectors are translocated into host cells to target various subcellular
258 compartments, manipulating diverse physiological and immune processes (Lo
259 Presti *et al.*, 2015). To determine the subcellular localization of XopN, we
260 expressed XopN-GFP in rice protoplasts. The fusion protein was primarily
261 localized to the plasma membrane (PM) and cytoplasm (Fig. 1f). Together,
262 these results demonstrate that XopN functions to dampen rice immune
263 responses at multiple levels, including callose deposition, ROS production, and
264 defense gene induction.

265 **XopN targets the scaffold protein OsRACK1B in rice**

266 To identify potential rice targets of XopN, we conducted a yeast two-hybrid (Y2H)
267 screen using a rice cDNA library with XopN as bait. This screen identified
268 OsRACK1B, a scaffold protein, as a putative interactor of XopN. To confirm this
269 preliminary interaction, full-length coding sequences of XopN and OsRACK1B
270 were cloned into the pGBKT7 (bait) and pGADT7 (prey) vectors, respectively.
271 Y2H assays confirmed that XopN interacts with OsRACK1B in yeast (Fig. 2a).
272 To further substantiate this interaction, we performed a reciprocal Y2H assay in

273 which full-length OsRACK1B was cloned into the pGBKT7 vector and XopN
274 into pGADT7. This reversed configuration also yielded a positive interaction
275 signal (Fig. 2a). To assess whether this interaction occurs in planta, we
276 performed a bimolecular fluorescence complementation (BiFC) assay in rice
277 protoplasts. Yellow fluorescence was observed only upon co-expression of
278 nYFP–XopN and RACK1B–cYFP (Fig. 2b), indicating a specific interaction
279 between the two proteins. Additionally, a pull-down assay was conducted to
280 validate the interaction in vitro. His-tagged XopN was specifically pulled down
281 by GST–RACK1B, but not by GST alone, further supporting the direct
282 interaction (Fig. 2c).

283 We next mapped the interaction domains between XopN and OsRACK1B
284 using the Y2H system. A series of XopN truncations fused to GAL4-AD were
285 co-expressed with BD-OsRACK1B in yeast. The results indicated that the C-
286 terminal region of XopN (amino acids 240–358) is necessary for the interaction
287 (Fig. 2d). Similarly, truncated OsRACK1B constructs were tested for their ability
288 to bind XopN, revealing that the WD7 domain alone was sufficient to mediate
289 the interaction (Fig. 2e). Together, these data demonstrate that XopN physically
290 interacts with OsRACK1B both in vivo and in vitro and that this interaction is
291 mediated by specific regions within each protein.

292 ***OsRACK1B* gene expression is upregulated upon *Xoc* infection**

293 OsRACK1B encodes a 336-amino-acid protein containing seven WD40 repeats,
294 a domain architecture highly conserved across eukaryotic organisms (Fig. S2a).
295 Phylogenetic analysis revealed that OsRACK1B shares the highest sequence
296 identity with its paralog OsRACK1A in rice (83.8%) and displays greater
297 similarity to orthologs in monocot species, including maize ZmRACK1 (82.5%)
298 and wheat TaRACK1A (80.5%), than to those in dicots such as tobacco
299 NtRACK1 (68.8%) and *Arabidopsis* AtRACK1C (68.4%) (Supplementary Figure
300 S4B). Moderate sequence conservation was also observed with human (61.7%)

301 and yeast (44.0%) RACK1 homologs (Fig. S2b), underscoring a deep
302 evolutionary relationship within the eukaryotic lineage. Notably, no RACK1
303 homologs have been identified in bacterial genomes, suggesting that RACK1
304 family proteins are unique to eukaryotes.

305 To determine whether *Xoc* infection alters *OsRACK1B* transcript levels, we
306 analyzed *OsRACK1B* mRNA abundance in rice leaves following inoculation
307 with the wild-type *Xoc* strain GX01. RT–qPCR revealed that *OsRACK1B*
308 expression was significantly induced at 12 and 24 hours post-inoculation (hpi)
309 (Fig. 3a), indicating transcriptional upregulation in response to pathogen
310 challenge. To examine whether this induction depends on the T3SS, we
311 examined *OsRACK1B* mRNA levels in rice leaves inoculated with a T3SS-
312 deficient mutant (Δ*hrcC*). The expression of *OsRACK1B* was induced to a
313 similar level compared to the leaves infected with GX01 (Fig. 3b), suggesting
314 that the induction of *OsRACK1B* is independent of the bacterial T3SS.

315 **OsRACK1B plays a positive role in rice resistance against *Xoc***

316 To determine the subcellular localization of OsRACK1B, we co-expressed
317 OsRACK1B-CFP with the nuclear marker ABF1-mCherry in rice protoplasts.
318 The CFP signal was observed in the plasma membrane, cytoplasm, and
319 nucleus (Fig. 3c), indicating that OsRACK1B is a multi-compartmental protein.
320 To further investigate the functional role of *OsRACK1B* in rice responses to *Xoc*,
321 we generated stable transgenic rice lines constitutively overexpressing
322 *OsRACK1B* under the control of the CaMV 35S promoter via *Agrobacterium*
323 *tumefaciens*-mediated transformation. A total of fifteen independent T_0
324 transgenic lines were confirmed by PCR and subsequently advanced to the T_2
325 generation. Among these, two independent homozygous overexpression lines,
326 designated RACK1BOE-2 and RACK1BOE-3, exhibited elevated OsRACK1B
327 transcript abundance compared to wild-type NIP plants and were selected for
328 subsequent functional analyses (Fig. 3d). To evaluate the impact of *OsRACK1B*

329 overexpression on BLS resistance, we inoculated transgenic and wild-type
330 plants with *Xoc* strain GX01. At 14 days post-inoculation (dpi), both RACK1BOE
331 lines displayed significantly reduced lesion lengths compared to wild-type
332 controls, indicative of enhanced resistance to *Xoc* infection (Fig. 3e,f).

333 We also generated *OsRACK1B* knockout mutants using CRISPR–Cas9-
334 mediated genome editing. Two independent knockout lines, OsRACK1BKO-2
335 and OsRACK1BKO-8, were identified. PCR amplification and sequencing
336 analysis revealed that OsRACK1BKO-2 carried a 2-bp deletion and a 1-bp
337 insertion at the U6a-gRNA and U6b-gRNA target sites, respectively, whereas
338 OsRACK1BKO-8 harbored a 1-bp insertion at both target sites (Fig. 4a).
339 Following GX01 inoculation, lesion lengths in the knockout plants were
340 significantly greater than those in wild-type controls (Fig. 4b,c). Together, these
341 findings indicate that *OsRACK1B* functions as a positive regulator of resistance
342 to BLS in rice.

343 **Knockout of *OsRACK1B* suppresses the rice immune response**

344 To gain mechanistic insights into the role of OsRACK1B in rice innate immunity,
345 we assessed callose deposition in *OsRACK1B* knockout mutants. Following
346 inoculation with the Δ*hrcC* mutant strain, the knockout lines exhibited a marked
347 reduction in callose accumulation in leaf tissues compared to wild-type plants
348 (Fig. 5a,b). In parallel, DAB staining indicated that Δ*hrcC*-induced ROS
349 production was substantially attenuated in the knockout mutants relative to the
350 wild type (Fig. 5c). To further explore the impact of *OsRACK1B* on immune
351 signaling, we quantified the transcript levels of two defense-related genes,
352 *OsPBZ1* and *OsPAL1*, in the mutant lines. RT–qPCR analysis revealed a
353 significant downregulation of both genes following Δ*hrcC* challenge in
354 OsRACK1B knockout plants compared to wild-type controls (Fig. 5d,e). These
355 observations suggest that OsRACK1B contributes to PTI by regulating callose
356 deposition, ROS accumulation, and defense gene expression.

357 **XopN impairs the OsRACK1B–OsRap2.6 interaction**

358 In order to explore the biological significance of the XopN–OsRACK1B
359 interaction, we investigated whether XopN influences the protein stability of
360 OsRACK1B. To this end, we assessed the accumulation of OsRACK1B–HA in
361 stable RACK1B-OE transgenic plants following inoculation with either the wild-
362 type GX01 or the Δ*xopN* mutant. Immunoblot analysis revealed no appreciable
363 change in OsRACK1B protein abundance (Fig. S3), indicating that XopN does
364 not affect OsRACK1B stability in planta.

365 The transcription factor OsRap2.6 plays a pivotal role in rice innate immunity
366 through its interaction with RACK1 (Wamaitha *et al.*, 2012; Yoshihisa *et al.*,
367 2022). In the present study, we first confirmed the physical association between
368 OsRap2.6 and OsRACK1B using Y2H assays (Fig. S4). Given that the bacterial
369 effector XopN also binds to OsRACK1B, we hypothesized that XopN might
370 modulate the OsRACK1B–OsRap2.6 interaction. Therefore, we first employed
371 AlphaFold3 prediction to investigate this hypothesis. The results showed that
372 the predicted interaction score between OsRACK1B and OsRap2.6 was 0.65,
373 which decreased substantially to 0.25 upon the addition of XopN, suggesting
374 that XopN may inhibit the interaction between OsRACK1B and OsRap2.6 (Fig.
375 6a). To validate this finding, we employed yeast three-hybrid (Y3H) assays to
376 assess the OsRACK1B–OsRap2.6 interaction in the presence of either full-
377 length. XopN or a truncated variant, XopN1–358. Notably, co-expression of
378 either form of XopN significantly attenuated the interaction between
379 OsRACK1B and OsRap2.6 (Fig. 6b). These findings suggest that XopN
380 competitively disrupts the association between OsRACK1B and OsRap2.6,
381 potentially interfering with downstream immune signaling.

382 ## Discussion

383 T3SEs are key virulence determinants in Gram-negative bacterial pathogens

384 that actively manipulate host cellular processes to promote infection(Kay &
385 Bonas, 2009). These effectors are known to specifically target host substrates,
386 thereby suppressing immunity and enhancing pathogen proliferation. In the
387 present study, we demonstrate that *Xoc* effector XopN facilitates bacterial
388 infection by targeting the rice scaffold protein OsRACK1B, a positive regulator
389 of innate immunity. During infection, XopN is translocated into host cells via the
390 T3SS and competes with OsRap2.6 for binding to OsRACK1B. This competitive
391 interaction leads to impaired immune signaling, as evidenced by reduced
392 callose deposition, attenuated ROS accumulation, and downregulation of
393 defense-related gene expression, thereby promoting successful colonization of
394 host tissues by *Xoc* (Fig. 6c).

395 To establish a successful infection, many host-adapted bacterial pathogens
396 deploy T3SEs that suppress plant immune responses from within host cells.
397 Previous research has demonstrated that *Xcv* effector XopN inhibits callose
398 deposition in both tomato and *Arabidopsis thaliana* (Kim *et al.*, 2009). In line
399 with these findings, we observed that XopN from *Xoc* also suppresses callose
400 accumulation in rice (Figure 1a,b), suggesting a conserved effector function
401 across diverse plant species. Moreover, XopN inhibited ROS generation and
402 downregulated the expression of defense-related genes (Fig. 1c-e). Collectively,
403 these data indicate that XopN enhances *Xoc* virulence by broadly attenuating
404 multiple layers of basal immune defense.

405 Phytopathogen effectors have evolved to subvert host immunity through
406 direct interactions with plant proteins, thereby undermining defense signaling
407 pathways (Dodds & Rathjen, 2010). In the present work, we provide multiple
408 lines of evidence by Y2H, in vitro pull-down and BIFC assays showing that
409 XopN interacts with the rice scaffold protein OsRACK1B (Figure 2). Previous
410 studies have shown that *Xcv* XopN is localized to both the PM and the
411 cytoplasm (Kim *et al.*, 2009). Our analysis of XopN localization in planta, using
412 transient expression of XopN-GFP in rice protoplasts, supports this finding (Fig.

413 1f). OsRACK1B is localized in the PM, cytoplasm, and nucleus (Supplementary
414 Fig. 3c), suggesting that the localization of OsRACK1B partially overlaps with
415 that of XopN in plant cells. However, whether the interaction between XopN and
416 OsRACK1B in these subcellular compartments is essential for full resistance
417 remains unclear. Future studies will be necessary to delineate the precise
418 subcellular locations of their interaction and further explore the molecular
419 functions of XopN in plant immunity.

420 In *Arabidopsis*, the three RACK1 homologs AtRACK1A, AtRACK1B, and
421 AtRACK1C have been implicated in a wide range of physiological processes,
422 including developmental regulation, hormone signaling, innate immunity, and
423 responses to abiotic stress (Chen *et al.*, 2006; Cheng *et al.*, 2015; Islas-Flores
424 *et al.*, 2015). Rice encodes two homologs, OsRACK1A and OsRACK1B. While
425 overexpression of OsRACK1A has been reported to promote ROS
426 accumulation and enhance resistance to *Ustilaginoidea virens* and
427 *Magnaporthe oryzae* (Nakashima *et al.*, 2008; Li *et al.*, 2022), the functional
428 role of OsRACK1B in immunity has remained largely unexplored. Here, we
429 show that OsRACK1B expression is transcriptionally upregulated during the
430 early stages of infection, as revealed by RT-qPCR analysis (Fig. 3a-b),
431 suggesting a role in basal defense against *Xoc*. This hypothesis was further
432 substantiated by resistance assays in OsRACK1B-overexpression and
433 knockout lines (Fig. 3 c-e and Fig. 4). Further functional analysis revealed that
434 OsRACK1B is essential for Δ*hrcC*-triggered callose deposition, ROS
435 production, and transcriptional activation of defense-related genes in rice (Fig.
436 5). Collectively, these findings identify OsRACK1B as a positive regulator of rice
437 immunity and suggest that it may serve as a critical node in the defense
438 signaling network against *Xoc* infection.

439 Scaffold protein RACK1 serves as a pivotal integrative hub in eukaryotes,
440 coordinating diverse signaling pathways through interactions with numerous
441 protein partners (Islas-Flores *et al.*, 2015; Fu *et al.*, 2024). Prior studies have

442 demonstrated that RACK1 forms a complex with the transcription factor Rap2.6,
443 a module implicated in rice immunity against *M. oryzae* (Wamaitha *et al.*, 2012;
444 Guo & Sun, 2017). More recently, OsRap2.6 has been shown to regulate NLR
445 Xa1-mediated immunity in response to TAL effector recognition, underscoring
446 its central role in pathogen resistance signaling (Yoshihisa *et al.*, 2022). Here,
447 we report that the *Xoc* effector XopN disrupts the interaction between
448 OsRACK1B and OsRap2.6 (Fig. 6a,b). However, the functional consequence
449 of this disruption on OsRap2.6 remains unclear. Based on structural and
450 functional considerations, we speculate that XopN may affect the stability or
451 transcriptional activity of OsRap2.6. This mechanism is reminiscent of the
452 interaction between *Xcv* effector XopN and the tomato proteins TFT1 and
453 TARK1, where XopN promotes the formation of TFT1-TARK1 complex (Kim *et*
454 *al.*, 2009; Taylor *et al.*, 2012). Notably, in contrast to the stabilizing effect
455 observed in tomato, XopN in rice appears to dismantle the OsRACK1B–
456 OsRap2.6 complex, suggesting a species-specific modulation by this
457 evolutionarily conserved effector. Structural elucidation of XopN would likely
458 reveal the molecular basis of its interaction with the OsRACK1B–OsRap2.6
459 subcomplex and offer mechanistic insights into its mode of action.

460 In conclusion, our findings reveal a potential pathogenic mechanism through
461 which *Xoc* type III effector XopN targets the rice scaffold protein OsRACK1B to
462 attenuate basal immunity and promote bacterial colonization. This work
463 deepens current understanding of non-TALE-mediated host–pathogen
464 interactions and holds implications for the development of disease-resistant rice
465 cultivars.

466 **Author contributions**

467 S.H. conceived the research and designed the experiments. J.W., Z.N., X.C.,
468 Y.Z. and H.Q. performed the experiments; J.W., Z.N. and H.W. analysed the
469 data. J.W. wrote the manuscript. S.H., J.T., and Y.H. revised the manuscript. All

470 authors have read and approved the final manuscript.

471 **Conflict of interest**

472 The authors declare no conflict of interest.

473 **Data availability statement**

474 All relevant data can be found within the manuscript and its supporting materials.

475 **Acknowledgments**

476 This research was supported by the National Natural Science Foundation of
477 China (31860032 and 32360045).

478

479 **References**

480 Boller T, He SY. 2009. Innate immunity in plants: an arms race between pattern
481 recognition receptors in plants and effectors in microbial pathogens. SCIENCE
482 324(5928): 742-744.

483 Cernadas RA, Doyle EL, Nino-Liu DO, Wilkins KE, Bancroft T, Wang L, Schmidt
484 CL, Caldo R, Yang B, White FF, Nettleton D, Wise RP, Bogdanove AJ. 2014.
485 Code-assisted discovery of TAL effector targets in bacterial leaf streak of rice
486 reveals contrast with bacterial blight and a novel susceptibility gene. PLoS
487 Pathogens 10(2).

488 Chen JG, Ullah H, Temple B, Liang J, Guo J, Alonso JM, Ecker JR, Jones AM.
489 2006. RACK1 mediates multiple hormone responsiveness and developmental
490 processes in Arabidopsis. JOURNAL OF EXPERIMENTAL BOTANY 57(11):
491 2697-2708.

492 Cheng Z, Li JF, Niu Y, Zhang XC, Woody OZ, Xiong Y, Djonovic S, Millet Y, Bush
493 J, McConkey BJ, Sheen J, Ausubel FM. 2015. Pathogen-secreted proteases
494 activate a novel plant immune pathway. NATURE 521(7551): 213-216.

Cui Y, Zou L, Zou H, Li Y, Zakria M, Chen G. 2013. HrpE3 is a type III effector protein required for full virulence of Xanthomonas oryzae pv. oryzicola in rice. MOLECULAR PLANT PATHOLOGY 14(7): 678-692.

Deb S, Ghosh P, Patel HK, Sonti RV. 2020. Interaction of the Xanthomonas effectors XopQ and XopX results in induction of rice immune responses. PLANT JOURNAL 104(2): 332-350.

Dodds PN, Rathjen JP. 2010. Plant immunity: towards an integrated view of plant-pathogen interactions. NATURE REVIEWS GENETICS 11(8): 539-548.

Fu Y, Zhu W, Zhou Y, Su Y, Li Z, Zhang D, Zhang D, Shen J, Liang J. 2024. RACK1a promotes hypocotyl elongation by scaffolding light signaling components in Arabidopsis. Journal of Integrative Plant Biology 66(5): 956-972.

Gao M, He Y, Yin X, Zhong X, Yan B, Wu Y, Chen J, Li X, Zhai K, Huang Y, Gong X, Chang H, Xie S, Liu J, Yue J, Xu J, Zhang G, Deng Y, Wang E, Tharreau D, Wang G, Yang W, He Z. 2021. Ca2+ sensor-mediated ROS scavenging suppresses rice immunity and is exploited by a fungal effector. CELL 184(21): 5391-5404.

Guo R, Sun W. 2017. Sumoylation stabilizes RACK1b and enhance its interaction with RAP2.6 in the abscisic acid response. Scientific Reports 7: 44090.

He Z, Zhang Z, Vale G, San SB, Chen X, Pasupuleti J. 2023. Editorial: disease and pest resistance in rice. Frontiers in Plant Science 14: 1333904.

Islas-Flores T, Rahman A, Ullah H, Villanueva MA. 2015. The receptor for activated c kinase in plant signaling: tale of a promiscuous little molecule. Frontiers in Plant Science 6: 1090.

Jones JD, Dangl JL. 2006. The plant immune system. NATURE 444(7117): 323-329.

521 Kay S, Bonas U. 2009. How Xanthomonas type III effectors manipulate the host
522 plant. CURRENT OPINION IN MICROBIOLOGY 12(1): 37-43.

523 Kim JG, Li X, Roden JA, Taylor KW, Aakre CD, Su B, Lalonde S, Kirik A, Chen
524 Y, Baranage G, McLane H, Martin GB, Mudgett MB. 2009. Xanthomonas t3s
525 effector XopN suppresses PAMP-triggered immunity and interacts with a
526 tomato atypical receptor-like kinase and TFT1. PLANT CELL 21(4): 1305-1323.

527 Leong JX, Raffeiner M, Spinti D, Langin G, Franz-Wachtel M, Guzman AR, Kim
528 JG, Pandey P, Minina AE, Macek B, Hafren A, Bozkurt TO, Mudgett MB, Bornke
529 F, Hofius D, Ustun S. 2022. A bacterial effector counteracts host autophagy by
530 promoting degradation of an autophagy component. EMBO JOURNAL 41(13):
531 e110352.

532 Li B, Meng X, Shan L, He P. 2016. Transcriptional regulation of pattern-triggered
533 immunity in plants. Cell Host & Microbe 19(5): 641-650.

534 Li GB, He JX, Wu JL, Wang H, Zhang X, Liu J, Hu XH, Zhu Y, Shen S, Bai YF,
535 Yao ZL, Liu XX, Zhao JH, Li DQ, Li Y, Huang F, Huang YY, Zhao ZX, Zhang JW,
536 Zhou SX, Ji YP, Pu M, Qin P, Li S, Chen X, Wang J, He M, Li W, Wu XJ, Xu ZJ,
537 Wang WM, Fan J. 2022. Enhanced production of OsRACK1a, an effector-
538 targeted scaffold protein that promotes OsRBOHB-mediated ROS production,
539 confers rice floral resistance to false smut disease without yield penalty.
540 Molecular Plant.

541 Li N, Lin Z, Yu P, Zeng Y, Du S, Huang L. 2023. The multifarious role of callose
542 and callose synthase in plant development and environment interactions.
543 Frontiers in Plant Science 14: 9.

544 Li S, Wang Y, Wang S, Fang A, Wang J, Liu L, Zhang K, Mao Y, Sun W. 2015.
545 The type III effector AvrBs2 in Xanthomonas oryzae pv. oryzicola suppresses
546 rice immunity and promotes disease development. MOLECULAR PLANT-
547 MICROBE INTERACTIONS 28(8): 869-880.

548 Liao Z, Li J, Mo X, Ni Z, Jiang W, He Y, Huang S. 2020. Type III effectors xopn
549 and avrBS2 contribute to the virulence of Xanthomonas oryzae pv. oryzicola
550 strain GX01. RESEARCH IN MICROBIOLOGY 171(2): 102-106.

551 Liu H, Lu C, Li Y, Wu T, Zhang B, Liu B, Feng W, Xu Q, Dong H, He S, Chu Z,
552 Ding X. 2022. The bacterial effector AvrRxo1 inhibits vitamin b6 biosynthesis to
553 promote infection in rice. Plant Communications 3(3): 100324.

554 Liu L, Li Y, Xu Z, Chen H, Zhang J, Manion B, Liu F, Zou L, Fu ZQ, Chen G.
555 2022. The Xanthomonas type III effector XopAP prevents stomatal closure by
556 interfering with vacuolar acidification. Journal of Integrative Plant Biology
557 64(10): 1994-2008.

558 Liu W, Liu J, Triplett L, Leach JE, Wang GL. 2014. Novel insights into rice innate
559 immunity against bacterial and fungal pathogens. Annual Review of
560 Phytopathology 52: 213-241.

561 Lo Presti L, Lanver D, Schweizer G, Tanaka S, Liang L, Tollot M, Zuccaro A,
562 Reissmann S, Kahmann R. 2015. Fungal effectors and plant susceptibility.
563 Annual Review of Plant Biology 66: 513-545.

564 Ma Z, Qin G, Zhang Y, Liu C, Wei M, Cen Z, Yan Y, Luo T, Li Z, Liang H, Huang
565 D, Deng G. 2021. Bacterial leaf streak 1 encoding a mitogen-activated protein
566 kinase confers resistance to bacterial leaf streak in rice. PLANT JOURNAL
567 107(4): 1084-1101.

568 Nakashima A, Chen L, Thao NP, Fujiwara M, Wong HL, Kuwano M, Umemura
569 K, Shirasu K, Kawasaki T, Shimamoto K. 2008. RACK1 functions in rice innate
570 immunity by interacting with the Rac1 immune complex. PLANT CELL 20(8):
571 2265-2279.

572 Oliva R, Ji C, Atienza-Grande G, Huguet-Tapia JC, Perez-Quintero A, Li T, Eom
573 JS, Li C, Nguyen H, Liu B, Auguy F, Sciallano C, Luu VT, Dossa GS, Cunnac S,
574 Schmidt SM, Slamet-Loedin IH, Vera CC, Szurek B, Frommer WB, White FF,

575 Yang B. 2019. Broad-spectrum resistance to bacterial blight in rice using
576 genome editing. NATURE BIOTECHNOLOGY 37(11): 1344-1350.

577 Robert X, Gouet P. 2014. Deciphering key features in protein structures with
578 the new ENDscript server. NUCLEIC ACIDS RESEARCH 42(Web Server
579 issue): W320-W324.

580 Spoel SH, Dong X. 2012. How do plants achieve immunity? Defence without
581 specialized immune cells. NATURE REVIEWS IMMUNOLOGY 12(2): 89-100.

582 Sun H, Zhu X, Li C, Ma Z, Han X, Luo Y, Yang L, Yu J, Miao Y. 2021.
583 Xanthomonas effector XopR hijacks host actin cytoskeleton via complex
584 coacervation. Nature Communications 12(1): 4064.

585 Taylor KW, Kim J, Su XB, Aakre CD, Roden JA, Adams CM, Mudgett MB. 2012.
586 Tomato TFT1 is required for PAMP-triggered immunity and mutations that
587 prevent t3s effector XopN from binding to TFT1 attenuate Xanthomonas
588 virulence. PLoS Pathogens 8(6): e1002768.

589 Triplett LR, Cohen SP, Heffelfinger C, Schmidt CL, Huerta AI, Tekete C, Verdier
590 V, Bogdanove AJ, Leach JE. 2016. A resistance locus in the American heirloom
591 rice variety Carolina Gold Select is triggered by TAL effectors with diverse
592 predicted targets and is effective against African strains of Xanthomonas oryzae
593 pv. oryzicola. PLANT JOURNAL 87(5): 472-483.

594 Tsuda K, Katagiri F. 2010. Comparing signaling mechanisms engaged in
595 pattern-triggered and effector-triggered immunity. CURRENT OPINION IN
596 PLANT BIOLOGY 13(4): 459-465.

597 Wamaitha MJ, Yamamoto R, Wong HL, Kawasaki T, Kawano Y, Shimamoto K.
598 2012. OsRap2.6 transcription factor contributes to rice innate immunity through
599 its interaction with receptor for activated kinase-c 1 (RACK1). Rice 5.

600 Wang J, Liao Z, Jin X, Liao L, Zhang Y, Zhang R, Zhao X, Qin H, Chen J, He Y,

601 Zhuang C, Tang J, Huang S. 2024. Xanthomonas oryzae pv. oryzicola effector
602 tal10a directly activates rice OsHXK5 expression to facilitate pathogenesis.
603 PLANT JOURNAL 119(5): 2423-2436.

604 Wang S, Li S, Wang J, Li Q, Xin XF, Zhou S, Wang Y, Li D, Xu J, Luo ZQ, He
605 SY, Sun W. 2021. A bacterial kinase phosphorylates OSK1 to suppress stomatal
606 immunity in rice. Nature Communications 12(1): 5479.

607 Wang W, Feng B, Zhou JM, Tang D. 2020. Plant immune signaling: advancing
608 on two frontiers. Journal of Integrative Plant Biology 62(1): 2-24.

609 Wang Y, Pruitt RN, Nurnberger T, Wang Y. 2022. Evasion of plant immunity by
610 microbial pathogens. NATURE REVIEWS MICROBIOLOGY 20(8): 449-464.

611 Xie H, Lin C, Lu W, Han Z, Wei D, Huo X, Li T, Zhang J, He Y, Chen C. 2023.
612 OsBLS6.2: a rice bacterial leaf streak resistance gene identified by GWAS and
613 RNA-seq. Crop Journal (2095-5421) 11(6).

614 Xie X, Chen Z, Cao J, Guan H, Lin D, Li C, Lan T, Duan Y, Mao D, Wu W. 2014.
615 Toward the positional cloning of qblsr5a, a QTL underlying resistance to
616 bacterial leaf streak, using overlapping sub-CSSLs in rice. PLoS One 9(4):
617 e95751.

618 Xie X, Ma X, Zhu Q, Zeng D, Li G, Liu YG. 2017. CRISPR-GE: a convenient
619 software toolkit for CRISPR-based genome editing. Molecular Plant 10(9):
620 1246-1249.

621 Yoshihisa A, Yoshimura S, Shimizu M, Sato S, Matsuno S, Mine A, Yamaguchi
622 K, Kawasaki T. 2022. The rice OsERF101 transcription factor regulates the NLR
623 xa1-mediated immunity induced by perception of TAL effectors. NEW
624 PHYTOLOGIST 236(4): 1441-1454.

625 Yuan S, Linquist BA, Wilson LT, Cassman KG, Stuart AM, Pede V, Miro B, Saito
626 K, Agustiani N, Aristya VE, Krisnadi LY, Zanon AJ, Heinemann AB, Carracelas

G, Subash N, Brahmanand PS, Li T, Peng S, Grassini P. 2021. Sustainable intensification for a larger global rice bowl. Nature Communications 12(1): 7163.

Zhang H, Sun B, Wu W, Li Y, Yin Z, Lu C, Zhao H, Kong L, Ding X. 2024. The MYB transcription factor OsMYBxoc1 regulates resistance to xoc by directly repressing transcription of the iron transport gene OsNRAMP5 in rice. Plant Communications 5(6): 100859.

Figure legends

Figure 1. XopN suppresses immune responses in rice. (a) Callose deposition in rice leaves at 72 hours post-inoculation with the *Xoc* wild-type strain GX01, the Δ*xopN* mutant, and the complemented strain CΔ*xopN*. Scale

650 bar, 100 μm. **(b)** Quantification of callose deposits per leaf. Data represent
651 means ± standard deviations, n=5. Asterisks denote statistically significant
652 differences between the Δ*xopN* mutant and either the wild-type or
653 complemented strain (**, $P < 0.01$, Student's *t*-test). **(c)** DAB staining of rice
654 leaves at 72 hours post-inoculation with GX01, Δ*xopN*, and CΔ*xopN*. **(d, e)**
655 Relative expression levels of *OsPBZ1* and *OsPAL1* in NIP rice at 24 hours post-
656 inoculation with GX01, Δ*xopN*, and CΔ*xopN*. Rice actin was used as an internal
657 control. Data represent means ± standard deviations, n = 3. Asterisks indicate
658 significant differences compared to wild-type or complemented strains (**, $P <$
659 0.01, Student's *t*-test). **(f)** Subcellular localization of XopN in planta. Rice
660 protoplasts were transfected with a construct expressing XopN fused to the N-
661 terminus of GFP (XopN-GFP). At 24 h post-transfection, fluorescence was
662 visualized by confocal laser scanning microscopy. Scale bars, 10 μm.

663 **Figure 2. XopN physically interacts with OsRACK1B. (a)** Y2H analysis
664 showing the interaction between XopN and OsRACK1B. Yeast strain Y2HGold
665 was co-transformed with the indicated plasmid combinations and cultured on
666 SD/-Leu-Trp and the selective medium SD/-Leu-Trp-His-Ade. Plates were
667 incubated at 30 °C for 3 days prior to imaging. The p53/T combination served
668 as a positive control, and Lam/T as a negative control. EV, empty vector control.
669 SD/-LW, SD/-Leu-Trp; SD/-LWHA, SD/-Leu-Trp-His-Ade. **(b)** BiFC assay
670 demonstrating the in vivo interaction of XopN with OsRACK1B in rice
671 protoplasts. XopN was fused to the N-terminal fragment of YFP (nYFP), and
672 OsRACK1B to the C-terminal fragment (cYFP). Reconstituted YFP
673 fluorescence was visualized by confocal microscopy 20 hours post-
674 transformation. Scale bar, 10 μm. EV, empty vector control. **(c)** In vitro pull-
675 down assay confirming the physical interaction between XopN and OsRACK1B.
676 Recombinant His-tagged XopN and GST-tagged OsRACK1B, expressed and
677 purified from *E. coli*, were subjected to pull-down using Ni-NTA resin. Bound
678 proteins were detected by immunoblotting with anti-GST and anti-His

679 antibodies. **(d)** Y2H assay showing the interaction between OsRACK1B and
680 truncated fragments of XopN. **(e)** Y2H assay demonstrating the interaction
681 between XopN and truncated variants of OsRACK1B. Yeast strain Y2HGold
682 was co-transformed with the indicated plasmid combinations and cultured on
683 SD/-Leu-Trp and the selective medium SD/-Leu-Trp-His-Ade. Plates were
684 incubated at 30 °C for 3 days prior to imaging. SD/-LW, SD/-Leu-Trp; SD/-LWHA,
685 SD/-Leu-Trp-His-Ade.

686 **Figure 3. Overexpression of *OsRACK1B* enhances rice resistance to *Xoc*.**
687 **(a, b)** Expression dynamics of *OsRACK1B* in rice leaves following inoculation
688 with the wild-type *Xoc* strain GX01 or the T3SS-deficient mutant strain Δ*hrcC*.
689 Rice actin was used as an internal control. Data represent means ± standard
690 deviations, n = 3. Asterisks indicate statistically significant differences (**, $P <$
691 0.01, Student's *t*-test). **(c)** Subcellular localization of OsRACK1B in planta. Rice
692 protoplasts were transfected with a construct expressing OsRACK1B fused to
693 the N-terminus of CFP (OsRACK1B-CFP) and co-expressed with the nuclear
694 marker ABF1-mCherry. Fluorescence was detected by confocal laser scanning
695 microscopy at 24 h post-transfection. Scale bars, 10 μm. **(d)** Relative
696 expression of *OsRACK1B* in wild-type NIP and transgenic overexpression lines.
697 Rice actin was used as an internal control. Data represent means ± standard
698 deviations, n = 3. Asterisks indicate statistically significant differences (**, $P <$
699 0.01, Student's *t*-test). **(e)** Phenotypes of lesion expansion in the NIP and
700 *OsRACK1B* overexpression lines at 14 days post-inoculation with GX01. **(f)**
701 Lesion lengths in the NIP and *OsRACK1B* overexpression lines at 14 days post-
702 inoculation with GX01. Data are displayed as boxplots with individual data
703 points. Error bars represent maximum and minimum values. Center line,
704 median; box limits, 25th and 75th percentiles. Asterisk indicate a significant
705 difference between the NIP and *OsRACK1B* overexpression lines (**, $P < 0.01$,
706 Student's *t*-test, n = 20).

707 **Figure 4. Loss of *OsRACK1B* function compromises rice resistance to**

708 ***Xoc*. (a)** Generation of *OsRACK1B* homozygous knockout mutants via
709 CRISPR-Cas9 editing. The schematic illustrates the *OsRACK1B* gene structure
710 and the targeted genomic locus. Blue nucleotides denote the protospacer
711 adjacent motif (PAM); red letters indicate inserted bases; hyphens represent
712 nucleotide deletions. **(b)** Phenotypes of lesion expansion in the NIP and
713 *OsRACK1B* edited mutants at 14 days post-inoculation with GX01. **(c)** Lesion
714 lengths in the NIP and *OsRACK1B* edited mutants at 14 days post-inoculation
715 with GX01. Data are displayed as boxplots. Error bars represent maximum and
716 minimum values. Center line, median; box limits, 25th and 75th percentiles.
717 Asterisks indicate a significant difference between the NIP and OsRACK1B
718 edited mutants (**, $P < 0.01$, Student's *t*-test, n = 20).

719 **Figure 5. *OsRACK1B* is required for rice immune responses to *Xoc.* (a)**
720 Callose deposition in wild-type NIP and *OsRACK1B* knockout lines at 48 hours
721 post-inoculation with Δ*hrcC*. Scale bar, 50 μm. **(b)** Quantification of callose
722 deposits per leaf in NIP and OsRACK1B knockout plants. Data represent
723 means ± standard deviations, n=5. Asterisks denote statistically significant
724 differences between NIP and *OsRACK1B* knockout lines (**, $P < 0.01$,
725 Student's *t*-test). **(c)** DAB staining showing hydrogen peroxide (H_2O_2)
726 accumulation in NIP and *OsRACK1B* knockout lines at 48 hours post-
727 inoculation with Δ*hrcC*. **(d, e)** Relative transcript levels of *OsPBZ1* and *OsPAL1*
728 in NIP and *OsRACK1B* knockout lines at 24 hours post-inoculation with Δ*hrcC*.
729 Rice *actin* was used as an internal control. Data represent means ± standard
730 deviations, n=3. Asterisks denote statistically significant differences between
731 NIP and *OsRACK1B* knockout lines (**, $P < 0.01$, Student's *t*-test).

732 **Figure 6. XopN competes with OsRap2.6 for binding to OsRACK1B. (a)**
733 AlphaFold predicts the effect of XopN on the OsRACK1B–Rap2.6 interaction.
734 **(b)** Y3H assay was performed to evaluate the competitive binding dynamics
735 between XopN and OsRap2.6 for OsRACK1B. Yeast strain Y2HGold was co-
736 transformed with the indicated plasmid combinations and cultured on SD/-Leu-

Trp-Met and the selective medium SD/-Leu-Trp-His-Ade-Met. Plates were incubated at 30 °C for 3 days prior to imaging. EV, empty vector control. SD/-LWM, SD/-Leu-Trp-Met; SD/-LWHAM, SD/-Leu-Trp-His-Ade-Met. **(c)** Schematic summary of XopN function in rice–*Xoc* interactions. During infection, the type III effector XopN is secreted by *Xoc* and translocated into rice cells, where it targets the scaffold protein OsRACK1B, a key component of rice immune signaling against *Xoc*. XopN binds to OsRACK1B in a manner that competitively interferes with the recruitment of the transcription factor OsRap2.6, thereby disrupting the formation of an OsRACK1B–OsRap2.6 immune complex. This disruption attenuates downstream immune responses, including callose deposition, ROS accumulation, and the transcriptional activation of defense-related genes, ultimately facilitating bacterial colonization of host tissue.

Supporting Information

Additional Supporting Information may be found online in the Supporting Information section at the end of the article.

Fig. S1. Sequence alignment of XopN and its homologs.

Fig. S2. Sequence analysis of OsRACK1B.

Fig. S3. XopN does not affect protein stability of OsRACK1B.

Fig. S4. Validation of the interaction between OsRACK1B and OsRap2.6.

Table S1 Primers used in this study.

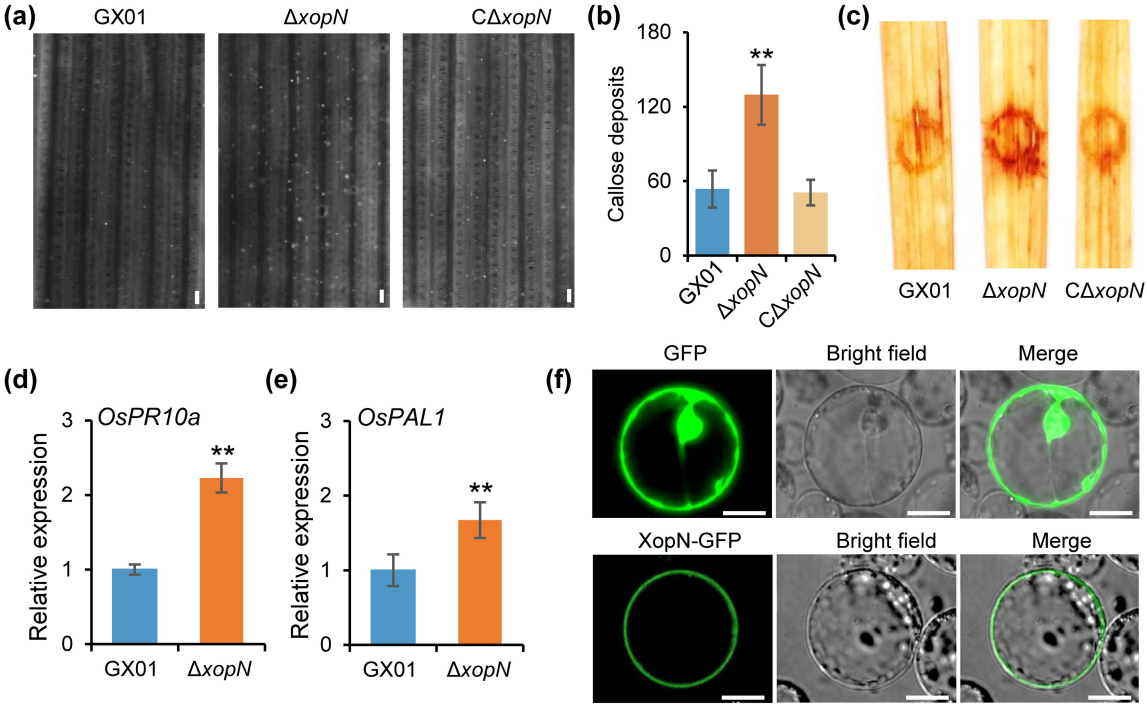
(a)
GX01
ΔxopN
CΔxopN
(b)
Callose deposits
180
120
60
0
**
GX01
ΔxopN
CΔxopN
(c)
GX01
ΔxopN
CΔxopN
(d)
OsPR10a
Relative expression
3
2
1
0
**
GX01
ΔxopN
(e)
OsPAL1
Relative expression
3
2
1
0
**
GX01
ΔxopN
(f)
GFP
Bright field
Merge
XopN-GFP
Bright field
Merge

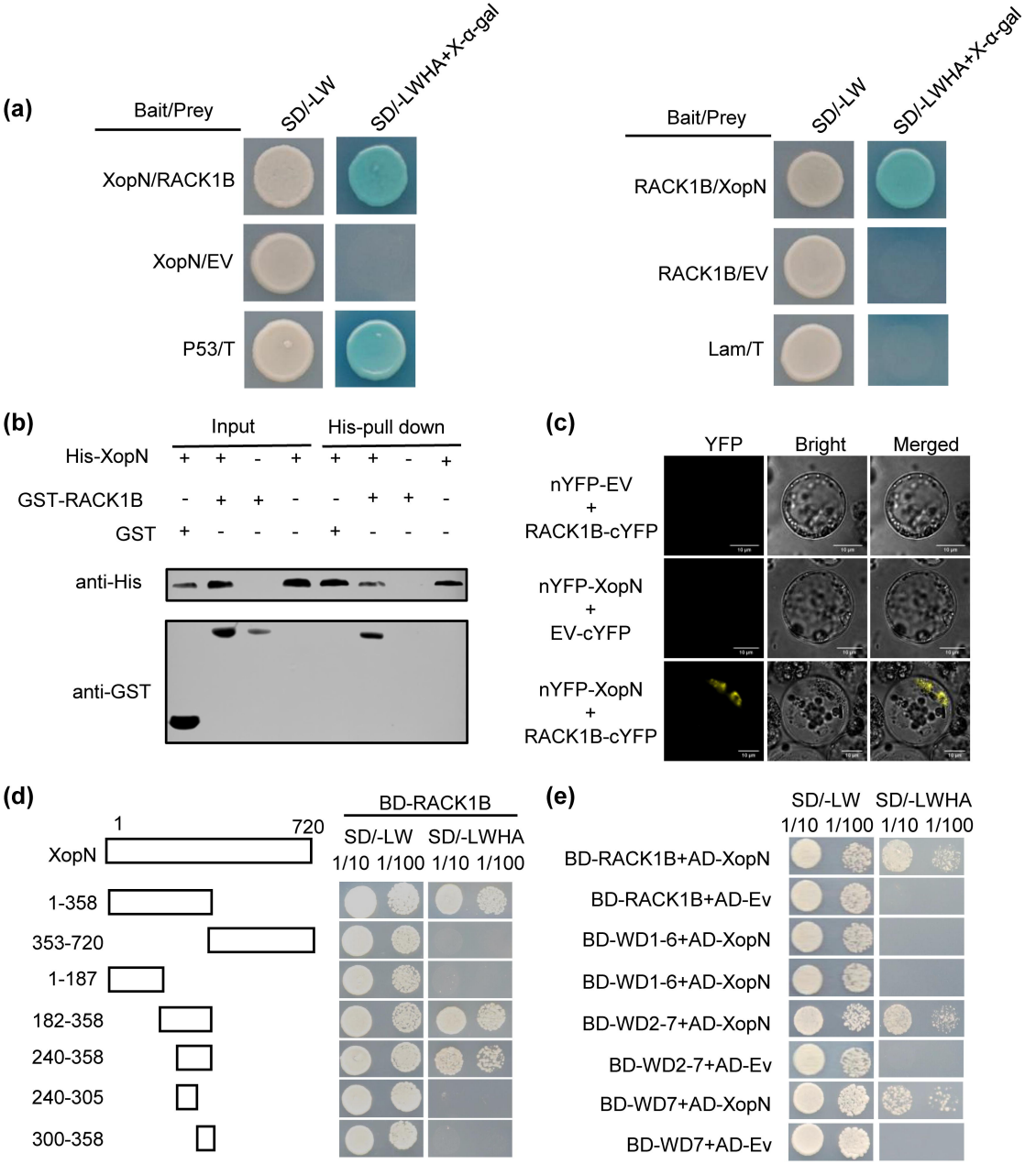
(a)
Bait/Prey
SD/-LW
SD/-LWHA+X-α-gal
XopN/RACK1B
XopN/EV
P53/T
Bait/Prey
SD/-LW
SD/-LWHA+X-α-gal
RACK1B/XopN
RACK1B/EV
Lam/T
(b)
Input
His-pull down
His-XopN + + - + + + - +
GST-RACK1B - + + - - + + -
GST + - - - + - - -
anti-His
anti-GST
(c)
YFP
Bright
Merged
nYFP-EV + RACK1B-cYFP
nYFP-XopN + EV-cYFP
nYFP-XopN + RACK1B-cYFP
(d)
BD-RACK1B
1
720
XopN
SD/-LW
SD/-LWHA
1/10 1/100 1/10 1/100
1-358
353-720
1-187
182-358
240-358
240-305
300-358
(e)
SD/-LW
SD/-LWHA
1/10 1/100 1/10 1/100
BD-RACK1B+AD-XopN
BD-RACK1B+AD-Ev
BD-WD1-6+AD-XopN
BD-WD1-6+AD-XopN
BD-WD2-7+AD-XopN
BD-WD2-7+AD-Ev
BD-WD7+AD-XopN
BD-WD7+AD-Ev

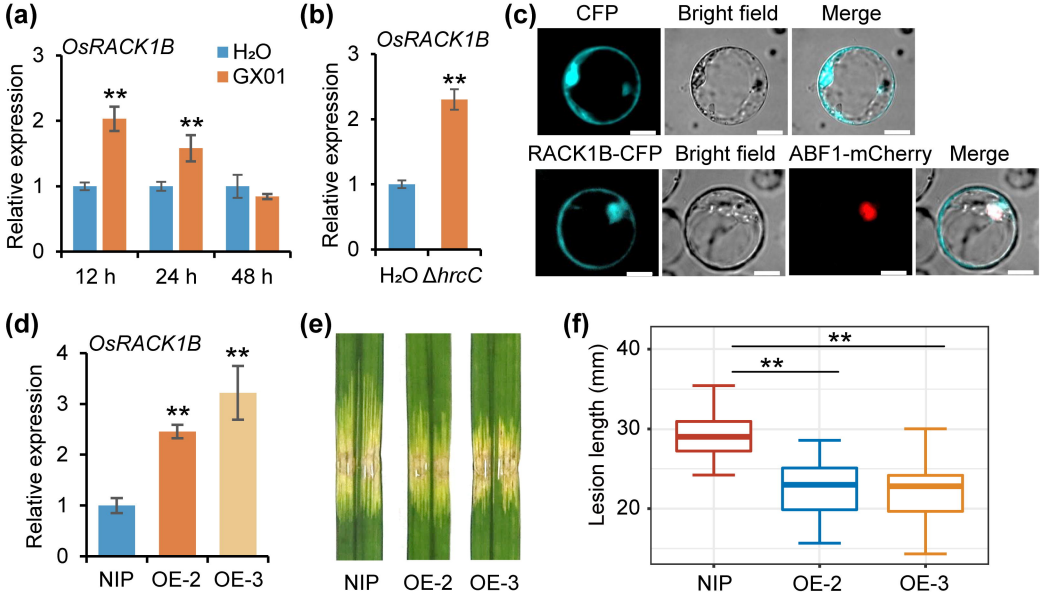
(a)
OsRACK1B
H₂O
GX01
Relative expression
0
1
2
3
**
**
12 h
24 h
48 h
(b)
OsRACK1B
Relative expression
0
1
2
3
**
H₂O
ΔhrcC
(c)
CFP
Bright field
Merge
RACK1B-CFP
Bright field
ABF1-mCherry
Merge
(d)
OsRACK1B
Relative expression
0
1
2
3
4
**
**
NIP
OE-2
OE-3
(e)
NIP
OE-2
OE-3
(f)
Lesion length (mm)
20
30
40
**
**
NIP
OE-2
OE-3

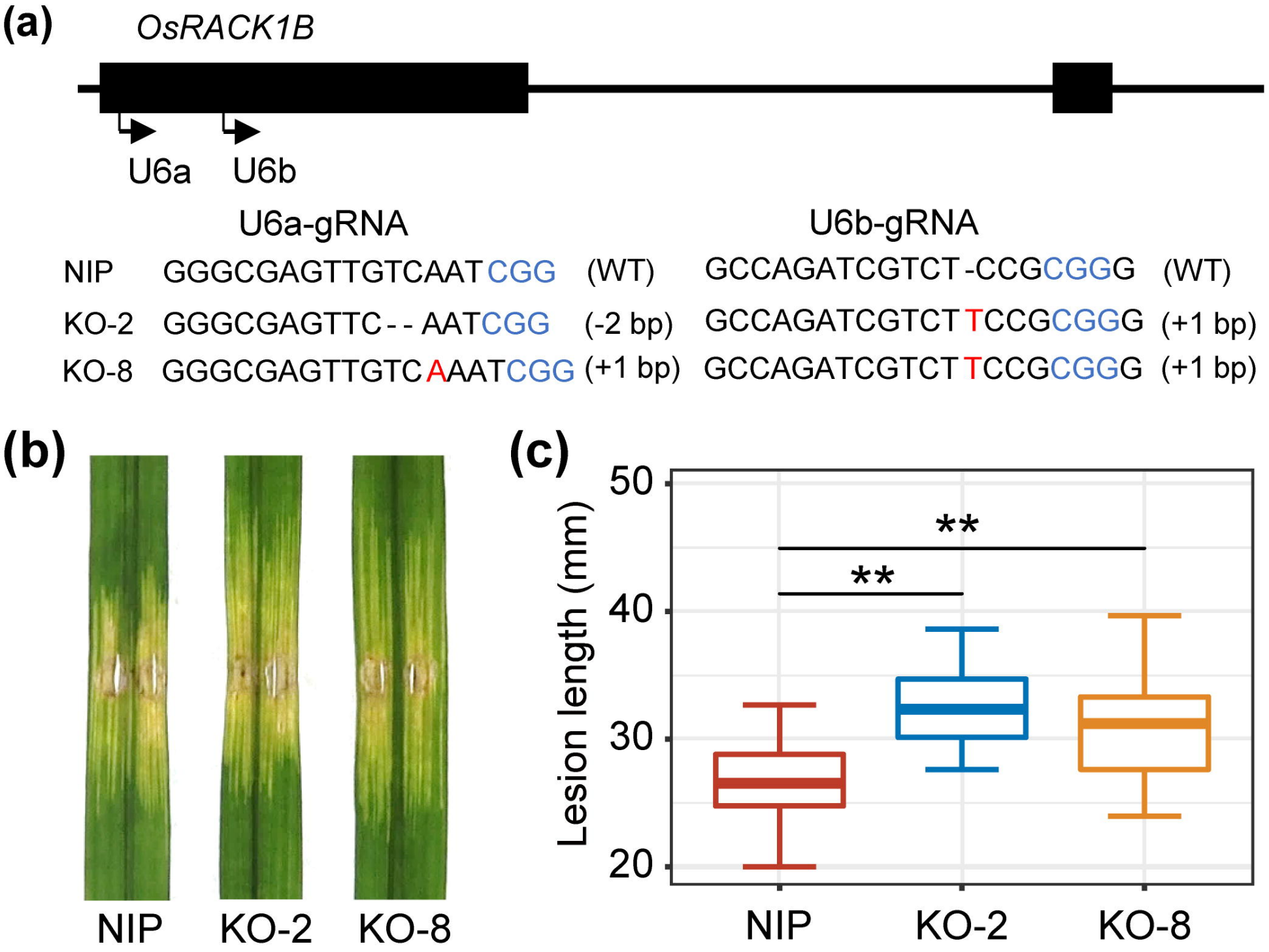
(a)
OsRACK1B
U6a
U6b
U6a-gRNA
U6b-gRNA
NIP GGGCGAGTTGTCAATCGG (WT) GCCAGATCGTCT-CCGCGGG (WT)
KO-2 GGGCGAGTTC--AATCGG (-2 bp) GCCAGATCGTCTTCCGCGGG (+1 bp)
KO-8 GGGCGAGTTGTCAAATCGG (+1 bp) GCCAGATCGTCTTCCGCGGG (+1 bp)
(b)
NIP
KO-2
KO-8
(c)
Lesion length (mm)
50
40
30
20
**
**
NIP
KO-2
KO-8

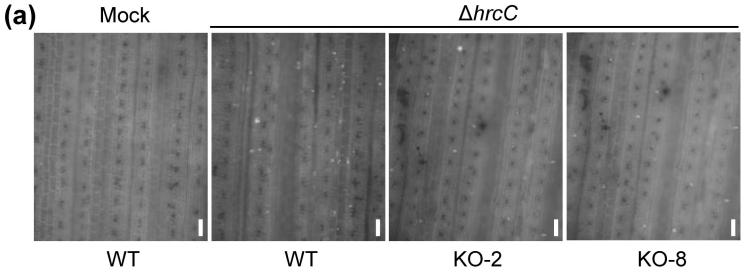
(a)
Mock
ΔhrcC
WT
WT
KO-2
KO-8

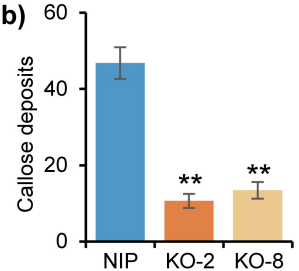
(b)
Callose deposits
60
40
20
0
**
**
NIP
KO-2
KO-8

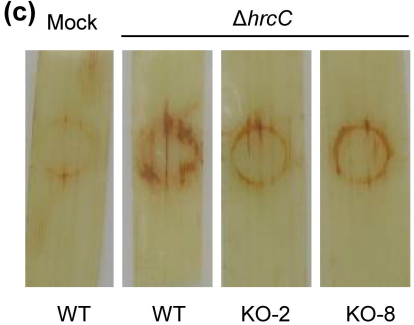
(c)
Mock
ΔhrcC
WT
WT
KO-2
KO-8

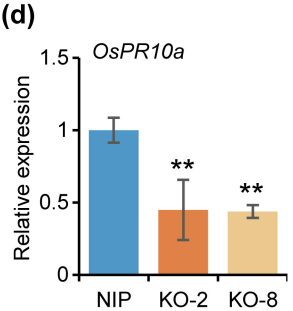
(d)
OsPR10a
Relative expression
1.5
1
0.5
0
**
**
NIP
KO-2
KO-8

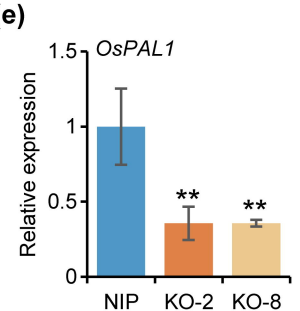
(e)
OsPAL1
Relative expression
1.5
1
0.5
0
**
**
NIP
KO-2
KO-8

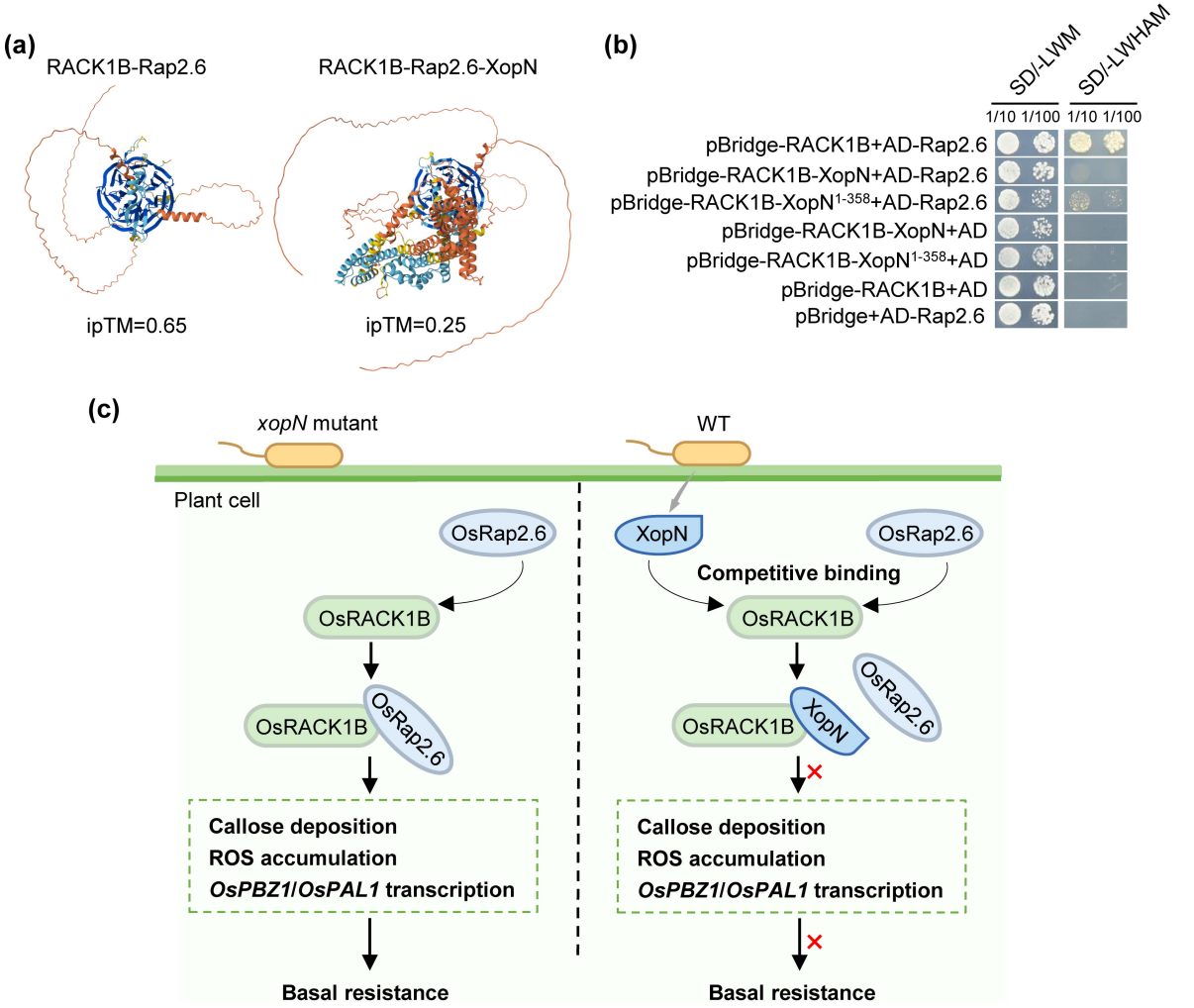
(a)
RACK1B-Rap2.6
RACK1B-Rap2.6-XopN
ipTM=0.65
ipTM=0.25
(b)
SD/-LWM
SD/-LWHAM
1/10 1/100 1/10 1/100
pBridge-RACK1B+AD-Rap2.6
pBridge-RACK1B-XopN+AD-Rap2.6
pBridge-RACK1B-XopN1-358+AD-Rap2.6
pBridge-RACK1B-XopN+AD
pBridge-RACK1B-XopN1-358+AD
pBridge-RACK1B+AD
pBridge+AD-Rap2.6
(c)
xopN mutant
WT
Plant cell
OsRap2.6
OsRACK1B
OsRACK1B
OsRap2.6
Callose deposition
ROS accumulation
OsPBZ1/OsPAL1 transcription
Basal resistance
XopN
OsRap2.6
Competitive binding
OsRACK1B
OsRACK1B
XopN
OsRap2.6
Callose deposition
ROS accumulation
OsPBZ1/OsPAL1 transcription
Basal resistance